TISSUE ENGINEERING: Part C
Volume 27, Number 11, 2021

DOI: 10.1089/ten.tec.2021.0178

termis
Tissue Engineering
& Regenerative Medicine
International Society

METHODS ARTICLE

Hyaluronic Acid-Functionalized Hybrid Gelatin–Poly-L-Lactide Scaffolds with Tunable Hydrophilicity

Germano Piccirillo, PhD,[1] Nora Feuerer, MSc,[1,2] Daniel A. Carvajal Berrio, MSc,[1,3] Shannon L. Layland, MBA,[1] Svenja Reimer Hinderer, PhD,[1,2] Brigida Bochicchio, PhD,[4] and Katja Schenke-Layland, PhD[1–3,5,i]

In this study, we describe the production of hybrid gelatin–poly-L-lactide electrospun scaffolds whose hydrophilicity was controlled by binding increasing concentrations of hyaluronic acid (HA). We show that cross-linking has advantages over coating when aiming to functionalize the scaffolds with HA. The here described scaffolds structurely mimicked the complexity of the extracellular matrix, and when excited by second harmonic generation, they produced a signal that is typical of collagen-containing biological fibers. Fluorescence lifetime imaging microscopy (FLIM) was used to marker-independently monitor the growth of human dermal fibroblasts on the electrospun scaffolds using reduced (phosphorylated) nicotinamide adenine dinucleotide as target. Benefitting from the different fluorescence lifetimes of the polymer and the endogenous cellular fluorophore, we were able to distinguish and separate the signals produced by the cells from the signals generated by the electrospun scaffolds. FLIM further allowed the detection of metabolic differences in the cells seeded on the HA-functionalized scaffolds compared with cells that were cultured on nonfunctionalized control scaffolds.

Keywords: electrospinning, fibroblasts, FLIM, Raman microspectroscopy, 3D cell culture, tissue engineering

Impact Statement

The study describes the production of hybrid gelatin–poly-L-lactide (GE:PLLA) electrospun scaffolds whose hydrophilicity was modified by cross-linking specific amounts of hyaluronic acid (HA) to the free amine residues of GE. Utilizing endogenous second harmonic generation signal and natural autofluorescence patterns as well as fluorescence lifetime imaging microscopy, we were able to marker independently and noninvasively monitor the seeded and unseeded electrospun scaffolds. The here presented data are highly relevant when aiming for the simultaneous *in vitro* imaging and metabolic analysis of cultured cells in an environment close to the physiological one, which is crucial for the *in vitro* testing of drugs, metabolites, and other bioactive molecules.

Introduction

Nanofibrillar electrospun scaffolds represent an emerging class of nanostructures that can mimic and reorganize the extracellular matrix (ECM) to sustain tissue regeneration and accelerate healing processes.[1–5] In the past years, growing attention has been paid to the advantages of hybrid scaffolds over single-component systems.[5–10] By combining two or more polymers, hybrid scaffolds are equipped with unique mechanical, biochemical, and structural properties.[9] Blend electrospun scaffolds have already been used in a wide range of tissue engineering and drug delivery systems.[7,10]

Electrospinning is a process that, starting from a polymer solution or melt, uses a high-voltage source to obtain three-dimensional (3D) structures composed of nanofibers and

[1]Institute of Biomedical Engineering, Department for Medical Technologies and Regenerative Medicine, Eberhard Karls University Tübingen, Tübingen, Germany.
[2]NMI Natural and Medical Sciences Institute at the University Tübingen, Reutlingen, Germany.
[3]Cluster of Excellence iFIT (EXC 2180) ''Image-Guided and Functionally Instructed Tumor Therapies,'' Eberhard Karls University Tübingen, Tübingen, Germany.
[4]Department of Science, University of Basilicata, Potenza, Italy.
[5]Department of Medicine/Cardiology, Cardiovascular Research Laboratories, David Geffen School of Medicine at UCLA, Los Angeles, California, USA.
[i]ORCID ID (https://orcid.org/0000-0001-8066-5157).

pores with variable sizes.[11–15] Electrospun scaffolds exhibit strong mechanical properties while maintaining a very high surface-to–volume ratio.[16,17] To date, the most widely used polymers to produce electrospun nanofibrous scaffolds are synthetic.[18,19] Among them, there are the polyesters polylactic acid,[20,21] polyglycolic acid,[22] and their copolymer, poly(lactic-coglycolic) acid.[23–25] All these materials are biocompatible and can be easily produced starting from inexpensive raw material sources.[20–26] To obtain biomimetic nano- and microfibers from such materials, an appealing approach has been the direct electrospinning of naturally derived polymers.[27–29]

To date, collagens, gelatin, fibrinogen, chitosan, and alginate have all been used as starting polymers to obtain nanofibrous structures by electrospinning.[29] Many of these macromolecules retain cell-binding sites and biomolecular signatures that can favor cell–material interactions.[25] However, the harvesting and processing of natural polymers are not as straightforward as for synthetic polymers, potentially impacting their unique and specific properties, or even causing denaturation.[25,26] Moreover, their poor miscibility with synthetic polymers can lead to badly blended polymeric nanofibers exhibiting unpredictable material properties because of inhomogeneity.[30–32] Thus, the production of hybrid electrospun nanostructures that can profit from the favorable biological properties of the natural polymer and the mechanical properties of the synthetic polymer remains a great challenge.

In this study, we present a method to develop and characterize hybrid electrospun scaffolds comprising well-blended gelatin (GE) and poly-L-lactide (PLLA) whose hydrophilicity was controlled by binding different amounts of HA. GE consists of a mixture of protein fragments, with a comparable amino acid composition as collagens, from which it derives through partial hydrolysis.[33]

Materials and Methods

GE has already been successfully employed in the production of biomaterials leveraging its biodegradability, biocompatibility, and commercial availability at low cost.[34] Mammalian GE is rich in domains able to bind to cell-surface receptors and to other ECM proteins, such as fibronectin, thus offering an excellent substrate for the attachment and proliferation of adherent cells.[35] In addition, GE can undergo collagenase-mediated hydrolysis, which allows the material resorption with no toxic residuals.[36] GE has advantages over collagens, such as collagen type I, which includes a lower immunogenicity[37–39] and a better solubility in aqueous systems.[40,41]

However, the high-water solubility of GE that represents an advantage for its processing makes the cross-linking mandatory before any use for biomedical applications. To date, carbodiimide-based cross-linking strategies represent the first choice.[42–46] The cross-linking reaction offers the possibility to specifically bind molecules to the amino acid residues.[47–50] PLLA is a widely used aliphatic polyester.[51] Cell adhesion for polylactide is not high due to its hydrophobicity,[52] but its mechanical strength and elasticity are much greater than GE.[53,54] PLLA can be chemically synthesized either by poly-condensation of lactic acid or by ring-opening polymerization of lactide, a cyclic dimer of lactic acid.[55] One of the very attractive properties of PLLA is that it can be resorbed *in vivo* after its hydrolytic or enzymatic digestion to the nontoxic lactic acid.[55] HA is a nonsulfated glycosaminoglycan (GAG) found within the ECM of human connective tissues consisting of the repetition of two alternating glycoside linkages of α-1, 4-D-glucuronic acid and β-1, 3-*N*-acetyl- D-glucosamine.[56]

HA is involved in tissue repair, wound healing, as well as cellular adhesion and proliferation.[57–61] A unique viscoelastic and rheological property together with its antibacterial and anti-inflammatory quality makes HA an attractive material for biomedical applications.[61] In addition, various proteins that impact ECM interactions can bind to HA, and thus it regulates how cells interact with their surrounding microenvironment.[62,63] The ECM serves, among other things, *in vivo* as a scaffold for cells and is responsible for cell proliferation, communication, and differentiation.[63,64] Blend nanofibrous electrospun scaffolds can mimic the complexity of the ECM of native tissues, and thus help to support cell adhesion and growth.[62]

The development of methodologies that allow the dynamic imaging and analysis of living cells and tissues in a neither invasive nor destructive way represents another great challenge. Multiphoton laser-based microscopy (MPM) has significantly enabled noninvasive bioimaging.[65] MPM is a technique based on nonlinear optical processes such as two-photon-excited fluorescence or second harmonic generation (SHG).[66]

The simultaneous absorption of two photons is very unlikely to occur and short-pulsed femtosecond lasers operating in the near infrared (NIR) are necessary.[67,68] Nevertheless, the usage of this kind of lasers offers many advantages when aiming to image biological samples. For example, relative low average powers (in the milliwatts range) are needed for the analysis since the excitation is limited to the focal point. At the same time, no absorption and fluorescence occur above and below the plane of focus and so photobleaching and phototoxicity are generally avoided.[68] Not least, the use of excitation wavelengths in the NIR (700 nm or even greater) makes this technique less biologically harmful and allows a deeper penetration depth into tissues or scattering samples when compared, for example, with confocal microscopy.[68]

Moreover, many endogenous biomolecules (e.g., reduced nicotinamide adenine dinucleotide or flavins) and biological structures, such as collagen and elastin fibers, generate autofluorescence or second harmonic signals after two-photon excitation at specific wavelengths, and so they do not need to be endogenously labeled.[65–69] These features make MPM a technique that allows quantitative high-resolution imaging of untreated/unlabled samples without manipulating or damaging them.[69] MPM has been employed for the *in vivo* evaluation of basal cell carcinoma.[68]

Other information can be obtained from each single pixel of an MPM acquisition if the system is specifically modified. Fluorescence lifetime imaging microscopy (FLIM) is a technique that can be coupled with MPM. FLIM allows, for example, the discrimination between fluorophores exhibiting different decay times,[67,68] or helps to attain information about cellular metabolism and biological microenviroments when having specific endogenous fluorophores as target molecules.[69]

All research was carried out in compliance with the rules for investigation of human subjects, as defined in the Declaration of Helsinki. The use of human fibroblasts in this study was approved by the local research Ethics Committee (F-2012-078).

Experiment

Experimental design

Electrospinning. PLLA (viscosity ~1.0 dL/g, 0.1% weight/volume (w/v) in chloroform (25°C), M_n 59,000, M_w 101 kDa, ester terminated) and GE (type B, from bovine skin, cell culture tested, M_w 50–100 kDa, bloom strength ~225 bloom) were purchased from Sigma-Aldrich (Steinheim, Germany). In total, 225 mg of PLLA was dissolved in 3 mL of 1,1,1,3,3,3-hexafluoro-2-propanol (Sigma-Aldrich) and the solution was incubated at 37°C under permanent magnetic stirring for 2 h. Thereafter, 225 mg of GE was added, and the solution was kept under magnetic stirring at 37°C for further 20 h.

Electrospinning experiments were performed with a customized electrospinning device.[70] An 18 G stainless steel needle was employed at a distance of 19 cm from the collector. Applied voltage and flowrate were 19.5 kV and 2.1 mL/h, respectively. Collagen type I from calf skin (Bornstein and Traub Type I, solid, BioReagent, suitable for cell culture) was purchased from Sigma-Aldrich. According to a reported literature protocol, the collagen was dissolved to a final concentration of 16% w% in a 1:1 v:v mixture of absolute ethanol (EtOH, EMD Merck Millipore, Darmstadt, Germany) and a 20X PBS buffer.[71] In this case, a 20 G stainless steel needle was employed at 10 cm from the collector. Applied voltage and flowrate were 20 kV and 1 mL/h, respectively.[71]

Cross-linking procedure. Sodium hyaluronate (95% degree of purity, molecular weight: 1.5 to 2.2 million Da) was purchased from ACROS Organics™ (part of Fisher Scientific GmbH, Schwerte, Germany). For the cross-linking, we used a solution in EtOH 95%/ddH_2O of *N*-(3-dimethylaminopropyl)-*N′*-ethylcarbodiimide hydrochloride (EDC·HCl, Novabiochem®, EMD Merck Millipore) and *N*-hydroxysuccinimide (NHS, Sigma-Aldrich) in equimolar ratio, both at the concentration of 50 mM.

Utilizing a 48-well plate (Greiner CELLSTAR™, Greiner Bio-One GmbH, Frickenhausen, Germany), punches of the electrospun scaffolds (9 mg, $\emptyset = 10$ mm) were immersed in 1 mL of the cross-linking mixture either supplied with or without HA. In total, 900 μL of EDC:NHS 50 mM:50 mM/EtOH 95% was added into each well. Then, 100 μL of either a sodium hyaluronate/ddH_2O solution or pure ddH_2O, as described by Yang *et al.*,[72] was added before immersing the scaffold punches. Sodium hyaluronate/ddH_2O solutions with different final w/v% (from 0.005% to 0.04%) were tested. After immersion, the scaffolds were incubated in the cross-linking mixture at room temperature (r.t.) for 24 h using an orbital shaker (60 rpm). The scaffolds were then gently dried on filter paper and washed with ddH_2O (3 × 1 mL ddH_2O) and finally kept in 1 mL of ddH_2O for another 24 h.

After the washing procedure, the excess water was removed using a filter paper. The scaffolds were finally immersed in 70% EtOH/ddH_2O for 30 min, then dried on filter paper, and allowed to stay overnight at r.t. to complete evaporation of any solvent residual.

HA coating. Punches (9 mg, $\emptyset = 10$ mm) of cross-linked GE:PLLA scaffolds in a 1:1 weight:weight (w:w) ratio were fully immersed in 1 mL of a 0.025% w/v HA solution in EtOH 85%/ddH_2O and gently mixed at r.t for 24 h using an orbital shaker (60 rpm). Thereafter, the solvent was let to completely evaporate overnight at r.t., and the scaffolds were used for further characterization either before or after being washed.

Cetrimonium bromide turbidimetric assay. HA conjugation onto electrospun scaffolds was confirmed and quantified by a reported indirect method using a cetrimonium bromide (CTAB, ≥98%, Sigma-Aldrich) turbidimetric assay.[73,74] The amount of conjugated HA was calculated by subtracting the amount in the supernatant fraction from the total amount used in the cross-linking reaction. In brief, after the cross-linking reaction (Section 2.2), skipping the washing steps, the solvent was allowed to completely evaporate. Then, 300 μL of 0.2 M sodium acetate (AcONa) buffer (pH 5.5), containing NaCl 0.15 M, was added into each well and the scaffolds were incubated at 37°C for 15 min. The same assay was performed for HA-coated scaffolds, either before or after the washing procedure.

A negative control (300 μL of 0.2 M AcONa +0.15 M NaCl) and a positive control (300 μL of 0.5 mg/mL sodium hyaluronate in 0.2 M AcONa +0.15 M NaCl) were also incubated at 37°C for 15 min. Afterward, 600 μL of 2.5% w/v CTAB solution in 2% w/v NaOH/ddH_2O was added into the wells, the scaffolds were removed, and the apparent absorbance of the insoluble complexes was measured within 10 min at 570 nm using a TECAN® Infinite 200 Reader (Crailsheim, Germany). The amount of unreacted or washed away HA was determined according to a linear calibration curve for HA concentrations between 0 and 0.5 mg/mL. Each sample was analyzed in sextuplicate.

Scanning electron microscopy. The morphology of the electrospun scaffolds was determined using a scanning electron microscope (1530 VP; Zeiss, Jena, Germany). After platinum sputter coating, images were acquired at a distance of 8 mm from the detector, a voltage of 15 kV, and different magnifications. The ImageJ® software supplied with the DiameterJ plug-in was used for fiber diameter and pores size analyses.

Contact angle measurements. Hydrophilicity of the electrospun substrates was analyzed using contact angle measurements with an OCA 40 device (DataPhysics Instruments GmbH, Filderstadt, Germany). A water drop with the volume of 2 μL was placed onto the sample and the contact angle was measured 10 s after water deposition using a video setup and the SCA20 software (DataPhysics Instruments) as previously described.[75] Results were calculated from 16 measurements obtained from four different scaffold pieces for each sample.

Uniaxial tensile testing. Electrospun scaffolds were cut into 10 × 20 mm rectangular pieces and clamped into the uniaxial tensile testing device (Electroforce 5500;

ElectroForce® Systems Group, Bose Corporation, MN, USA). The exact sample dimensions were determined before each measurement and recorded with the software for further calculations of Young's modulus and the tensile strength. The scaffolds were pulled to failure by applying a stretch of 0.025 mm/s. Young's modulus was calculated from the initial linear slope of the stress versus strain curve for each measurement. Measured values are presented as average ± standard deviation from 16 measurements obtained from four different scaffold pieces for each sample.

Swelling test analysis. For each sample, 16 different punches (9 mg, $\varnothing = 10$ mm) obtained from four different scaffolds were used. Each scaffold piece was immersed in 1 mL ddH_2O for 1 h at r.t. using an orbital shaker (60 rpm). In case water drops were clearly visible on the scaffold surface, the excess water was gently removed using filter paper. The rate of water absorbed by each piece was calculated according to the following formula [Eq. (1)][76]:

$$\text{Swelling } (\%) = \frac{\text{wet scaffold w (mg)} - \text{dry scaffold w (mg)}}{\text{dry scaffold w (mg)}} \times 100. \quad (1)$$

Formula used for the swelling test.[76]

Cell culture and seeding. This study was carried out in accordance with the institutional guidelines and was approved by the local research ethics committee (F-2012-078). Human dermal fibroblasts (HDFs) were isolated by enzymatic digestion as previously described.[77,78] Cells were cultured in Dulbecco's modified Eagle medium (DMEM, with L-glutamine; Gibco™, Life Technologies GmbH, Darmstadt, Germany) supplemented with 10% fetal calf serum (FCS; PAA Laboratories, Pasching, Austria) and 1% penicillin/streptomycin (100 U/mL penicilium and 100 μg/mL streptomycin, Life Technologies GmbH) in an incubator at 37°C and in a 5% CO_2 atmosphere.

Cell culture medium was changed every 3 days and cells were passaged or seeded using trypsin-EDTA (15090046, PAA Laboratories) at ~70% confluence. When seeding the cells directly on electrospun scaffolds, HDFs were seeded at a rate of 2×10^5 per cm^2. Scaffolds were rinsed with fresh culture medium 4 h after seeding.

In vitro cytotoxicity assay. According to an ISO 10993-5 accredited protocol, HDFs were exposed to an extract of the samples. The electrospun scaffolds were sterilized with 70% ethanol for 30 min. Then 6 cm^2 of each sample was incubated in 1 mL FCS- and antibiotic-free DMEM for 72 h. Each extract was prepared in triplicate. HDFs seeded in 96-well plates (2000 cells per well) were then exposed for 24 h to the extracts supplied with 10% FCS.

The extraction medium was removed, the cells were washed twice with phosphate buffer saline 1X (PBS, Gibco by Life Technologies GmbH), and a tetrazolium salt (3-(4,5-dimethylthiazol-2-yl)-5-(3-carboxymethoxyphenyl)-2-(4-sulfophenyl)-2H-tetrazolium [MTS]) assay (CellTiter 96Aqueous One Solution Cell Proliferation Assay, Promega, Mannheim, Germany) was performed as per the manufacturer's protocol. In brief, 20 μL of MTS solution was added to 100 μL of the scaffold's extracts. After 35 min incubation at 37°C, the absorbance of each well was measured at 492 nm using a TECAN® Infinite 200 Reader. The test was performed for a blind, a negative control (DMEM +10% v FCS), and a sodium dodecyl sulfate (Life Technologies GmbH, 1% w/v in DMEM)-treated positive control. For analysis, the negative control was set to 100%.

Raman microspectroscopy. The inverse Raman system and acquisition parameters used in this study were previously described.[79] In brief, a 784 nm diode laser with an output laser power of 85 mW was focused through a water-immersion objective (60X, NA 1.2, Olympus, Tokyo, Japan). The total acquisition time per spectrum was 100 s (10×10 s acquisitions). All Raman spectra were analyzed in the range from 400 to 1800/cm. Spectra were background subtracted, baseline corrected using OPUS (Bruker Optics, Ettlingen, Germany), and vector normalized using Unscrambler × 10.3 (Camo, Oslo, Norway) as previously described.[79]

Principal component analysis (PCA) was performed using Unscrambler × 10.3 to reduce spectral variables and identify spectral differences among the compared samples. Seven PCs were calculated for each PCA. PC loadings were considered in detail to identify the molecular components that were relevant for the comparison of the spectra.

MPM. Imaging was performed using a custom-built MPM system with a titanium–sapphire femtosecond laser (MaiTai XF1, Spectra Physics, Santa Clara) as previously described.[80] To evaluate triple-helix content of GE in the electrospun scaffolds, we defined a parameter [SAI, second harmonic to autofluorescence index, Eq. (2)] similar to the second harmonic to autofluorescence aging index of the dermis (SAAID).[81]

$$\text{SAI}(\%) = \frac{\text{SHG GVI}}{(\text{SHG GVI} + \text{AF GVI})} \times 100. \quad (2)$$

Formula used to evaluate the SHG to autofluorescence index (SAI).

In detail, an excitation wavelength of 760 nm and a laser power of 18 mW were employed, whereas a 380/20 band-pass emission filter and a 435 nm long pass filter were used to detect SHG and autofluorescence, respectively. For the mean gray value intensity analysis, ImageJ was used as software to process and analyze the images. For scaffold imaging, punches ($\varnothing = 10$ mm) of the scaffolds were rinsed with PBS 1X, put on Ibidi® (Ibidi GmbH, Planegg/Martinsried, Germany) glass-bottomed dishes (35 mm) and carefully pressed on the bottom with a cover glass before analysis.

Fluorescence lifetime imaging microscopy. FLIM was performed to assess reduced (phosphorylated) nicotinamide adenine dinucleotide (NAD(P)H) or GE mean fluorescence lifetime using time-correlated single photon counting (TCSPC) at an excitation wavelength of 710 nm and a laser power of 18 mW. HDF morphology was assessed on glass-bottomed dishes (Ibidi, 35 mm) with a density of 5×10^4 cells per dish.

After 24 h, the medium was removed and 2 mL of fresh DMEM (+10% FCS) was added. When the cells were imaged on the scaffolds, HDFs were analyzed 24 h after seeding. Before imaging, the electrospun scaffolds were flipped and carefully pressed on the bottom with a cover glass before analysis. FLIM data were recorded at an acquisition time of 180 s for 512×512 pixels with 64 time channels. The instrument response function was recorded using urea crystals (Sigma-Aldrich) at an excitation wavelength of 920 nm and a laser power of 4.5 mW for 120 s. The FLIM images were analyzed using the SPCImage software (Becker &Hickl GmbH, Berlin, Germany).

A biexponential decay fitting model [Eq. (3)] was employed at each pixel since NAD(P)H has two different lifetimes represented by τ_1 and τ_2.[80,82] A $\chi^2 < 1.1$ was accepted for a good fitting. For GE analysis, the mean fluorescence lifetime [τ_m] after the biexponential decay fitting was instead considered. A binning factor of 5 was used in the analysis. For each sample, four different dishes were used, and six images were acquired per dish.

$$I(t) = \alpha_1 e^{-\tau_1} + \alpha_2 e^{-\tau_2} + C. \quad (3)$$

Biexponential decay fitting used for the FLIM analysis. τ_1 represents the free NAD(P)H lifetime, whereas τ_2 the protein bound NAD(P)H lifetime.

Data analysis. All the reported graphs were plotted using Microsoft™ Excel. All data are presented as mean ± standard deviation ($n = 4$, unless stated otherwise in the Materials and Methods section). Statistical significance was determined by a Student's two-tailed unpaired *t*-test. $p \leq 0.05$ (*) was defined as statistically significant.

Results and Discussion

Scaffolds production and morphological characterization

In the first part of the study, we aimed to functionalize hybrid GE:PLLA electrospun scaffolds with HA. We performed GE cross-linking in the presence of different HA concentrations using a modified procedure from Yang *et al.*[72] In addition, a simple HA coating of previously cross-linked GE:PLLA scaffolds was performed. We tested different increasing HA concentrations and discovered that when using a HA w/v% >0.025 HA, the cross-linking solution appeared turbid with the formation of HA precipitates.

This observation reflected also in the final HA amount in the hybrid cross-linked scaffolds, which was quantified using an indirect CTAB-based turbidimetric assay (Fig. 1A). Interestingly, we observed a linear correlation between the HA w/v% in the cross-linking mixture and its final amount in the scaffold if it was <0.025% (Fig. 2A). When using higher HA concentrations, a plateau was reached on the y axis (scaffolds HA w% = 2.2% ± 0.1%, Fig. 2A), suggesting that the excess of HA simply precipitates in the cross-linking solution as we already observed macroscopically.

This observation also reflected on the microscopic level according to the scanning electron microscopy (SEM) images (Fig. 2B–G). Particularly by binding increasing HA amounts, we preserved the fibrous high-porous structure typical of the electrospun mats (Fig. 2B–F) until a value of 2.2 w% (Fig. 2G). When having this final HA w%, a film formed on the superficial fibers, likely due to the deposition of some precipitated HA during the cross-linking reaction. A similar behavior was observed when performing a simple HA coating on the GE:PLLA scaffolds (Fig. 1B). In this case, the effect was even more pronounced with a quite homogeneous film forming on the scaffold surface (Fig. 1B).

When washing the HA-coated samples using the standard procedure as for the cross-linked scaffolds, the superficial film disappeared and the electrospun scaffolds regained a more typical morphology (Fig. 1C). We concluded that this was due to HA slowly dissolving on the scaffold surfaces during the incubation in ddH_2O. This hypothesis was confirmed by the results of the CTAB assay, detecting no traces of HA in the coated scaffolds after the washing step (a.w., Fig. 1A). The described observations were confirmed in the observed fiber diameter distribution (Fig. 1D–K). When binding a HA w% not higher than 2 to the hybrid scaffolds, they all showed a normal fiber diameter distribution, with a mean value ~450 nm (Fig. 1D–H), and no significant difference when compared with the pure GE:PLLA scaffolds (in all cases $p > 0.6$).

When binding instead a HA 2.2 w% or when performing a HA coating, the fiber distribution was more spread (Fig. 1I, J). Interestingly, the coated samples regained a normal fiber distribution after washing, but the mean diameter was shifted toward the right probably due to a mechanical stress after the HA film deposition (Fig. 1K).

Physical properties of the hybrid scaffolds

After having functionalized the GE:PLLA scaffolds with a quantifiable amount of HA and having investigated their morphology, we evaluated their physical properties by measuring their elastic modulus (Fig. 3A), ultimate tensile strengths (UTS, Fig. 3B), contact angles (Fig. 4), and swelling properties in water (Fig. 3C). The HA addition affected neither the elastic modulus nor the UTS of the hybrid GE:PLLA scaffolds (Fig. 3A, B). Only after being washed, the HA-coated samples (a.w.) showed a significantly lower elastic modulus when compared with the pure GE:PLLA (elastic modulus GE:PLLA = 8.6 ± 0.6 MPa vs. a.w. = 10.8 ± 0.7 MPa, $p = 0.0041$) or the unwashed coated samples (HA coated = 8.2 ± 0.6 MPa vs. a.w. = 10.8 ± 0.7 MPa, $p = 0.0023$).

This observation was in accordance with the results of the SEM analysis, where we observed a loss in fiber elasticity as well as a change in the mean fiber diameters (Fig. 1C, K). Despite the addition of a high hydrophilic hygroscopic HA, the swelling properties in ddH_2O of the HA-functionalized scaffolds did not significantly change when compared with the pure GE:PLLA scaffolds. We hypothesize that the amount of HA is too low to affect this property with a prevalent effect and impact of the porosity of the structure as well as of the high content in the water-uptaking GE. Only the HA-coated scaffolds showed a significantly higher swelling percentage (GE:PLLA = 121% ± 9% vs. HA coated = 150% ± 11%, $p = 0.0021$), indicating an initial water uptake by the HA deposed on the scaffold surface.

However, after a longer incubation, the absorbed HA dissolved, not being retained anymore, so that the scaffold

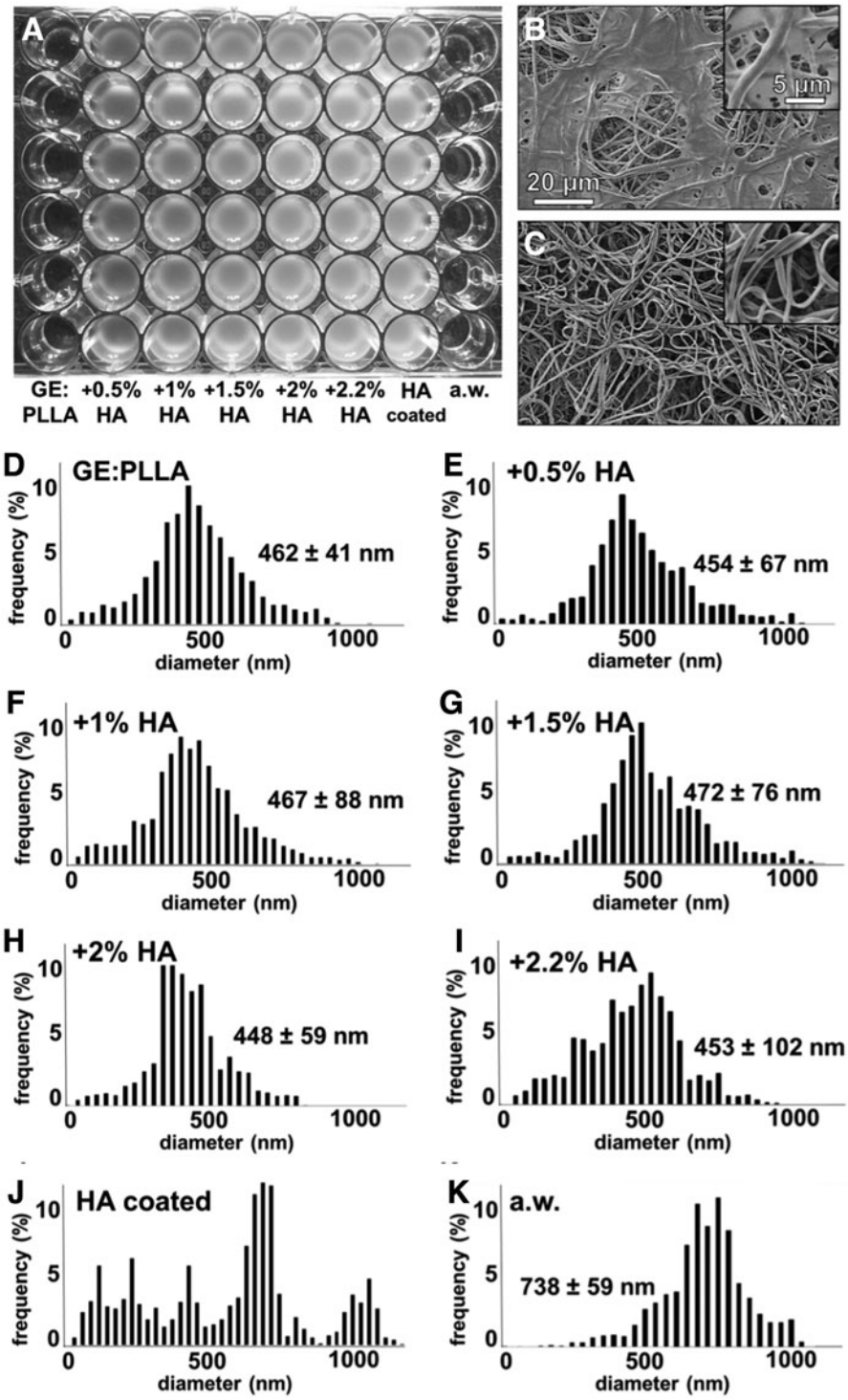

FIG. 1. **(A)** Results of the CTAB assay on the electrospun cross-linked hybrid GE:PLLA 1:1 scaffolds, either functionalized or not with HA. **(B, C)** SEM images at different magnifications **(B)** of HA-coated cross-linked electrospun GE:PLLA 1:1 either before (**B**) or after **(C)** 24 h incubation in ddH_2O by 37°C. **(D–K)** Fiber diameter distribution **(C)** of electrospun cross-linked GE:PLLA 1:1 (**D**); GE:PLLA 1:1 containing 0.5% w of HA (+0.5% HA, **E**); GE:PLLA 1:1 containing 1% w of HA (+1% HA, **F**); GE:PLLA1:1 containing 1.5% w of HA (+1.5% HA; **G**); GE:PLLA 1:1 containing 2% w of HA (+2% HA, **H**); GE:PLLA 1:1 containing 2.2% w of HA (+2.2% HA, **I**); GE:PLLA 1:1 coated with HA (HA coated, **J**); GE:PLLA 1:1 coated with HA after 24 h incubation in ddH_2O by 37°C (a.w., **K**). CTAB, cetrimonium bromide; GE:PLLA, gelatin–poly-L-lactide; HA, hyaluronic acid; SEM, scanning electron microscopy.

showed a swelling percentage that was not significantly different from the pure GE:PLLA (GE:PLLA = 121% ± 9% vs. a.w. = 127% ± 9%, $p = 0.42$). Nevertheless, the HA functionalization helped tune the scaffolds' hydrophilicity according to the contact angle measurements (Fig. 4). Surface liquid permeability is affected by many different aspects such as material composition, type of structure, porosity, roughness, capillarity, as well as surface tension, and interest has been raised by researchers within the past years to predict and control surface wettability.

Interestingly, we observed a linear correlation between the HA weight percentage in the scaffolds and their contact angle values (Fig. 4H). We identified that by each increasing HA amount, we could significantly decrease the scaffold's hydrophobicity (Fig. 4H, GE:PLLA = 129 ± 3° vs. +0.5% HA = 106 ± 7°, $p = 0.0034$; +0.5% HA = 106 ± 7° vs. +1%

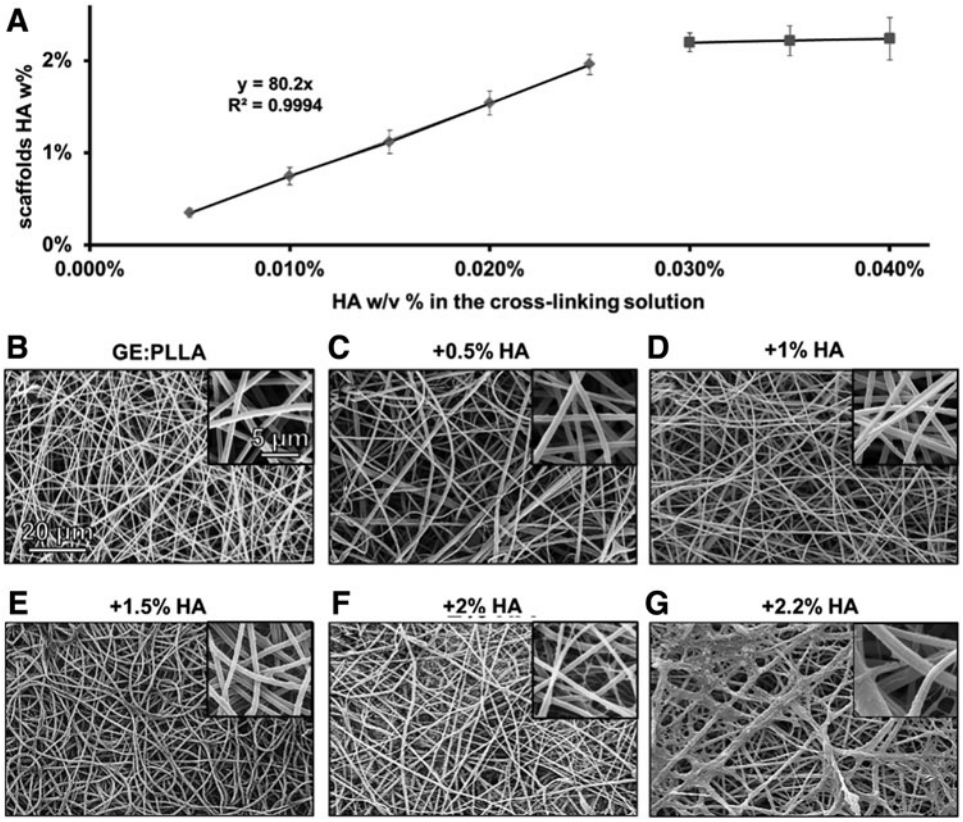

FIG. 2. **(A)** Linear correlation between the HA concentration used in the cross-linking reaction and the final HA amount in the hybrid GE:PLLA 1:1 scaffolds. When using a concentration >0.025% w/v, HA was not soluble anymore and a plateau is reached. **(B–G)** SEM images at different magnifications of the electrospun cross-linked hybrid GE:PLLA 1:1 scaffolds, either not functionalized or functionalized with HA. **(B)** GE:PLLA 1:1. **(C)** GE:PLLA 1:1 containing 0.5% w of HA (+0.5% HA). **(D)** GE:PLLA 1:1 containing 1% w of HA (+1% HA). **(E)** GE:PLLA 1:1 containing 1.5% w of HA (+1.5% HA). **(F)** GE:PLLA 1:1 containing 2% w of HA (+2% HA). **(G)**. GE:PLLA 1:1 containing 2.2% w of HA (+2.2% HA).

HA = 87 ± 10°, $p = 0.0086$; +1% HA = 87 ± 10° vs. +1.5% HA = 68 ± 11°, $p = 0.021$; +1.5% HA = 68 ± 11° vs. +2% HA = 53 ± 9°, $p = 0.032$).

The scaffolds coated with HA were the most hydrophilic ones, showing a contact angle that was significantly lower when compared with all the other samples (HA coated = 36 ± 3°, $p < 0.05$ in all cases), which may also be due to its higher swelling percentage (Fig. 3C). However, the HA-coated samples returned highly hydrophobic after the washing procedure, with contact angle values that did not significantly differ from those of pure GE:PLLA (GE:PLLA = 129 ± 3° vs. a.w. = 126 ± 4°, $p = 0.73$).

Raman microspectroscopy

The presence of HA in the hybrid electrospun scaffolds was also spectroscopically investigated with Raman microspectroscopy, which represents a marker-independent nondestructive technology for the detection of specific chemical bonds and groups.[66,77,79] We used a specific HA signal related to the spectral vibrations of the β-linkages at 894/cm[83–85] to detect the increasing HA amounts in the hybrid scaffolds. In the normalized spectra, the relative intensity of this signal was increasing with the increasing amount of HA in the scaffolds (Fig. 5A, B). The peak at 894/cm narrowed with the increasing HA weight percentage, thus supporting its identification, despite that it partially overlaped with a signal at 895/cm related to the C-COO stretching of the polyester PLLA.[86–88]

We performed a PCA to confirm these observations. First, we performed PCA to compare the hybrid GE:PLLA scaffolds that were cross-linked either without or with HA (Fig. 5C, D). For the loadings, the peak at 894/cm was the most relevant, with a contribution >80% (PC-1, 82%, Fig. 5D). Plotting this component on the x-axes of the PCA score graph, we identifed a shift toward the right with a higher contribution of the peak at 894/cm, which was due to the increasing HA content in the samples (Fig. 5C). We performed the same analysis to evaluate the presence of HA in the coated GE:PLLA scaffolds, both before and after the washing steps (Fig. 5E, F).

We identified that the most relevant component for the loadings was the one including the peak at 894/cm, which was identified as belonging to HA (PC-1, 79%, Fig. 5F). Our results suggest that although the coating protocol allowed the GE:PLLA functionalization with HA, this macromolecule was completely dissolved in the aqueous medium after only a single day of incubation. Thus, based on our Raman microspectroscopy results, we conclude that the cross-linking procedure offers an advantage over a simple coating for the GE:PLLA functionalization when aiming to obtain HA-functionalized scaffolds for long-term studies.

MPM of the scaffolds

We previously observed that electrospinning allows the regeneration of a collagen-like SHG signal from commercial GE when using a fluorinated alcohol as solvent.[89] This signal was stronger when blending GE together with PLLA.[89] The best results were achieved when mixing the two polymers together in an equal ratio.[89] Here, we aimed to

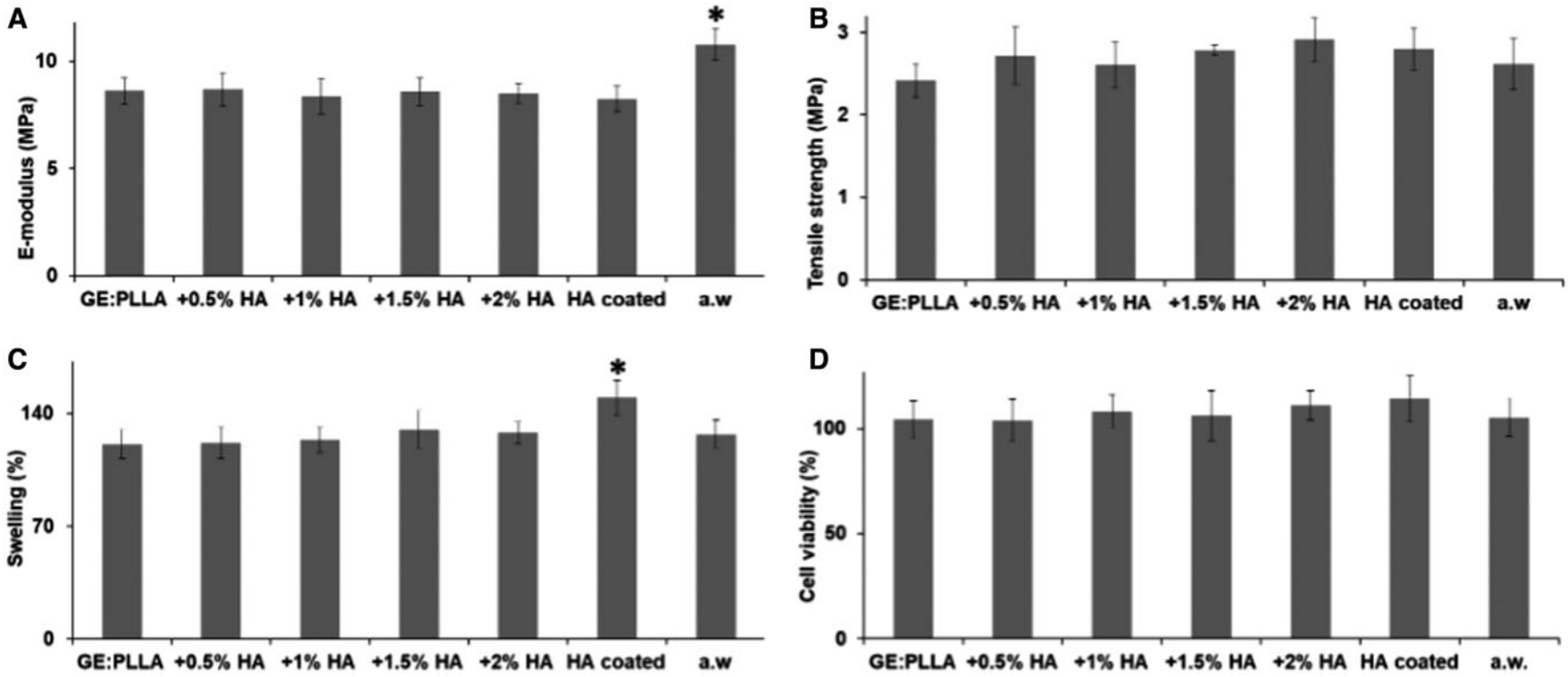

FIG. 3. Properties of the electrospun cross-linked hybrid GE:PLLA 1:1 scaffolds, either not functionalized or functionalized with HA. **(A, B)** Young's modulus (E-modulus, **A**) and ultimate tensile strength (**B**). **(C)** Water swelling percentage. **(D)** Results of the MTS assay. Proliferation >80% is noncytotoxic. MTS, 3-(4,5-dimethylthiazol-2-yl)-5-(3-carboxymethoxyphenyl)-2-(4-sulfophenyl)-2H-tetrazolium.

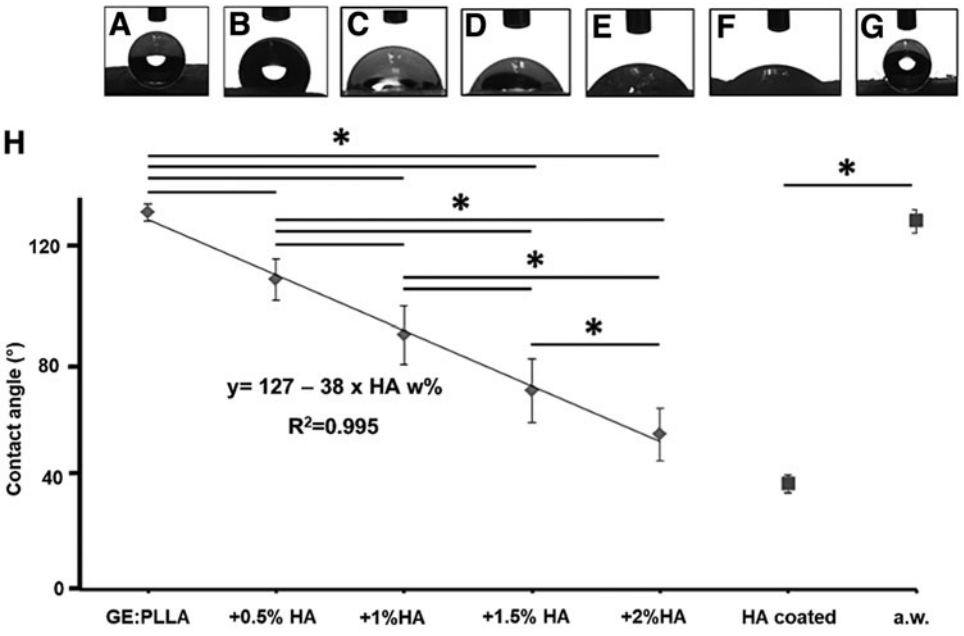

FIG. 4. **(A–G)** Snapshots from the drop shape analysis of the scaffolds. **(A)** GE:PLLA 1:1. **(B)** GE:PLLA 1:1 containing 0.5% w of HA (+0.5% HA). **(C)** GE:PLLA 1:1 containing 1% w of HA (+1% HA). **(D)** GE:PLLA 1:1 containing 1.5% w of HA (+1.5% HA). **(E)** GE:PLLA 1:1 containing 2% w of HA (+2% HA). **(F)** GE:PLLA 1:1 coated with HA (HA coated). **(G)** GE:PLLA 1:1 coated with HA after 24 h incubation in ddH_2O by 37°C (a.w). **(H)** Contact angle values for the electrospun cross-linked hybrid GE:PLLA 1:1 scaffolds. A linear correlation ($R^2 = 0.995$) was identified between the HA amount in the scaffolds and the values for the contact angle. $^*p \leq 0.05$ is significant

verify whether this property could be preserved when functionalizing GE:PLLA with HA. First, we recorded the SHG signals from pure collagen type I electrospun samples, spun using a benign solvent system that allows the retaining of a triple-helix structure and, thus, of a SHG signal in the electrospun fibers (Fig. 6A), as it was previously reported by Zeugolis *et al.*[90] and Dong *et al.*[71]

As expected, the presence of increasing amounts of HA did not alter the SHG signal of the GE:PLLA electrospun scaffolds, which was also comparable with the one composed of pure collagen type I (Fig. 6A–F). We also investigated the mean fluorescence lifetime τ_m of the scaffolds that may be influenced by the scaffold morphology and composition.[89,91–93] Interestingly, we observed a shift toward shorter τ_ms with an increasing HA content in the scaffolds, which is in accordance with a previous study of Fukushima *et al.*[94] on the glycation of collagen. However, we identified no significant difference even when comparing the τ_m of pure GE:PLLA with that of scaffolds containing the highest HA percentage (GE:PLLA = 2.22 ± 0.11 ns vs. +2% HA = 2.16 ± 0.14 ns, $p = 0.41$).

Pure collagen type I scaffolds showed instead the longest mean fluorescence lifetime, but a significant difference could be only found when comparing its τ_m with that of the hybrid scaffolds having the highest HA content (collagen = 2.26 ± 0.10 ns vs. +2% HA = 2.16 ± 0.14 ns, $p = 0.019$). This result is not surprising since collagen fluorescence lifetime is strongly affected by aging and cross-linking among others,[95,96] and thus is not directly comparable with that of GE.[97] Nevertheless, in all the other cases, the obtained τ_m values for the hybrid scaffolds were not significantly different when compared with pure collagen type I containing scaffolds. This aspect, together with the possibility of retaining an SHG signal, suggests that the electrospinning of GE together with PLLA and its subsequent functionalization with HA may represent a cheaper less affording alternative to the direct electrospinning of collagen type I.

FLIM assessment of the glycolytic activity of HDFs cultured on the hybrid scaffolds

We verified the biocompatibility of the hybrid scaffolds with a routine MTS-based cytotoxicity assay (in all cases cell viability was >100%, Fig. 3D), and then used FLIM to image HDFs seeded on the hybrid scaffolds. Besides cell imaging, FLIM enabled the measurement of the HDF glycolytic activity by assessing the ratios between free and protein-bound NAD(P)H.[80,98–100] We imaged and analyzed HDFs seeded on the GE:PLLA scaffolds containing the highest HA percentage (+2% HA) and compared these data with results obtained from HDFs seeded on either glass, electrospun collagen type I, or on GE:PLLA scaffolds without HA functionalization (Fig. 7A–P). As we could already observe in a previous study,[89] despite the strong autofluorescence of GE, we were able to distinguish cells from the scaffolds by a false color coding, based on a two-dimensional (2D) correlation using a biexponential decay curve fitting [Eq. (3)]. Particularly, the cellular NAD(P)H showed much shorter τ_1 and τ_m [Eq. (4)] values than those of electrospun collagen or GE.

$$\tau_m = \alpha_1(\%)\tau_1 + \alpha_2(\%)\tau_2. \quad (4)$$

Formula for the mean fluorescence lifetime of a biexponential decay fitting.

No differences were found for the τ_2 values (Fig. 7Q). Based on the 2D correlation, HDFs were colored in yellow, due to shorter fluorescence lifetimes, whereas scaffold fibers were colored in blue (Fig. 7A–D). Looking at the plotting with τ_1 and τ_m as variables on the x and y axes, the pixels obtained from the HDFs can be found in the lower left part of the plot, whereas those that are due to material contributions are in the upper right part (Fig. 7E–H). Based on these observations, we developed a spreadsheet using Microsoft Excel™ that allowed us to isolate all the pixels occupying either the lower left part of the 2D correlation

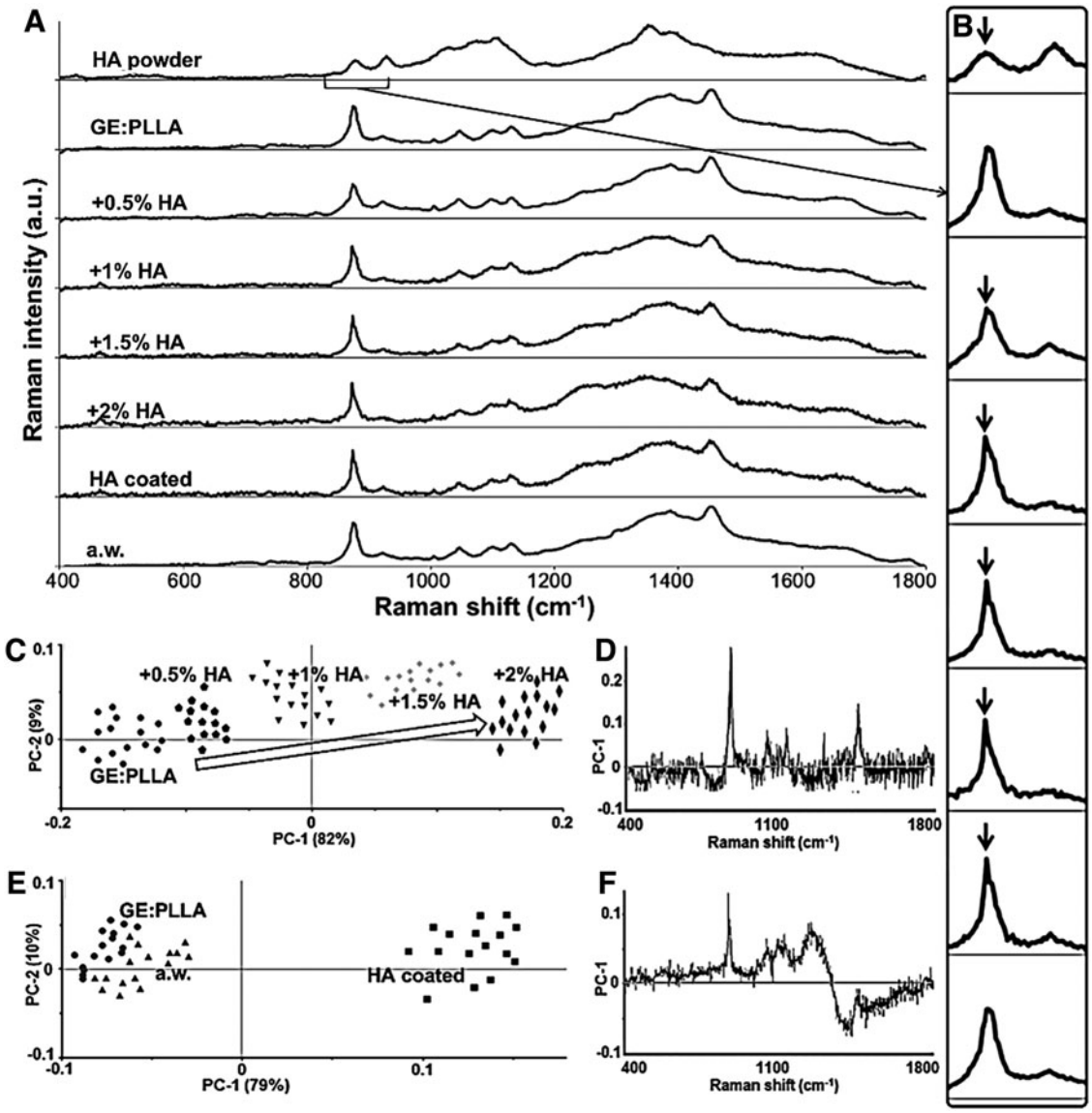

FIG. 5. **(A)** Raman spectra of pure HA and of the electrospun cross-linked hybrid GE:PLLA 1:1 scaffolds. **(B)** Zoom of the Raman spectra in the regions of interest showing a peak allowing the detection of HA (*arrow*). **(C)** Score graph after PCA analysis including the hybrid GE:PLLA 1:1 scaffolds after cross-linking in presence or not of HA, showing a separation with the increasing HA concentration (*arrow*). **(D)** Loadings for PC-1: the wavenumber with high (absolute) loading is identified as belonging to HA (894/cm). **(E)** Score graph after PCA of the hybrid cross-linked GE:PLLA 1:1 scaffolds, showing a separation after the HA coating. After 24 h incubation in ddH_2O by 37°C (a.w.), the samples cannot be clearly separated from the pure GE:PLLA 1:1 scaffolds (*left* part of the score graph) **(F)**. Loadings for PC-1. The wavenumber with highest (absolute) loading is identified as belonging to HA (894/cm). PCA, principal component analysis.

(τ_1 <1000 ps and τ_m <1750 ps, Fig. 7I–L) or the upper right part (τ_1 >1000 ps and τ_m >1750 ps, Fig. 7M–P).

Thereafter, we took the pixels in the lower left part of the plotting, belonging to the HDFs to analyze the free NAD(P)H ratio α_1 (%) and thus to detect metabolic shifts between glycolysis and oxidative phosphorylation.[80,98–100] According to the results (Figs. 7R and 8), only the HDFs seeded on the hybrid scaffolds with the highest HA content showed a lower glycolytic activity in terms of α_1 (%) when compared with HDFs seeded on glass (glass = 74 ± 5% vs. +2% HA = 61 ± 5%, $p = 0.003$), collagen type I scaffolds (collagen = 68 ± 5% vs. +2% HA = 61 ± 5%, $p = 0.009$), or pure GE:PLLA scaffolds (GE:PLLA = 69 ± 5% vs. +2% HA = 61 ± 5%, $p = 0.007$). No significant differences were found when comparing the other samples among each other (in all cases $p > 0.25$).

We conclude from our data that only HA significantly impacts the metabolic activity of the HDFs grown on the HA-functionalized scaffolds, showing an increase in the contribution of the protein-bound NAD(P)H to the final α_1 (%) ratio. It is well known that HA has a key role in protecting different cell lines from oxidative stress,[101–103] and it is well used as a therapeutic agent against pain that can be associated with inflammatory states.[104–107] Even if it has been for a long

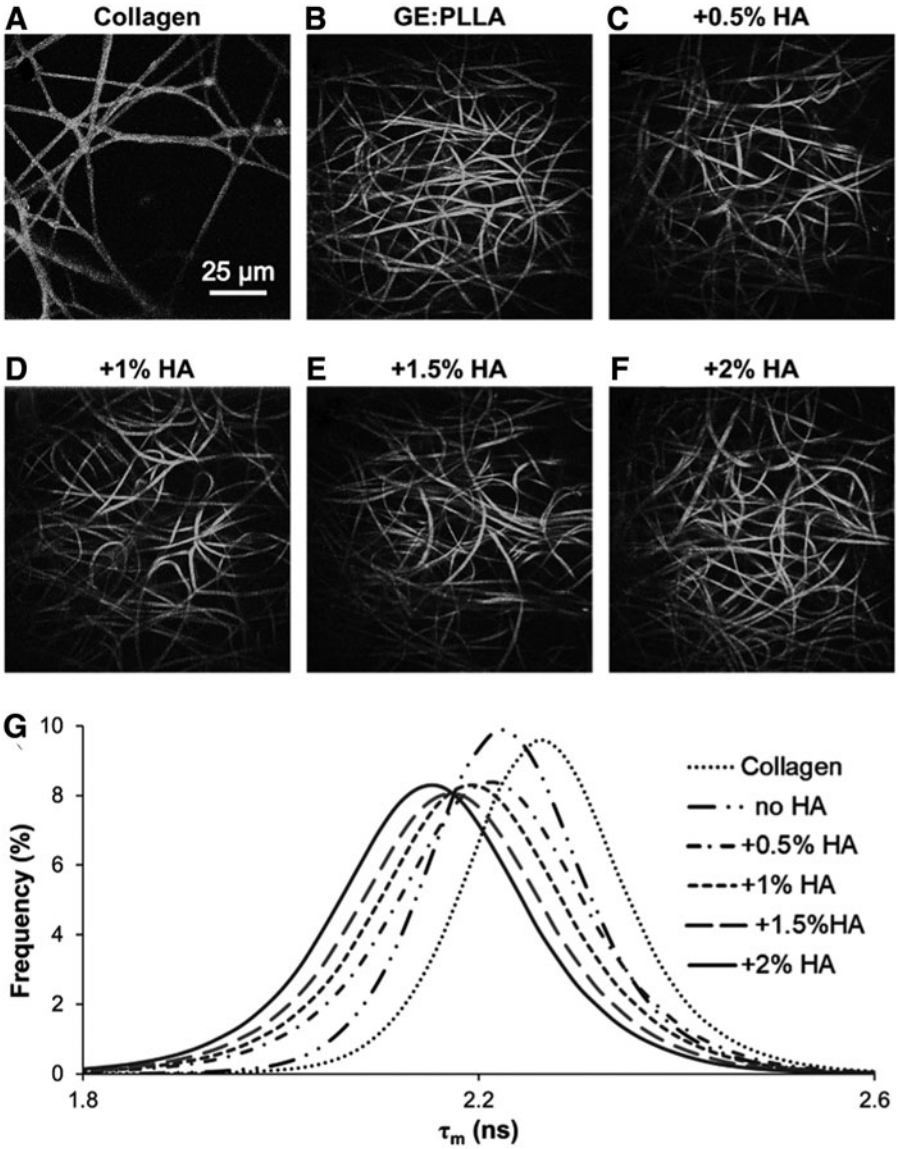

FIG. 6. **(A–E)** Second harmonic generation images of electrospun collagen **(A)**, cross-linked electrospun GE:PLLA 1:1 **(B)**, cross-linked electrospun GE:PLLA 1:1 containing 0.5% w of HA (+0.5% HA, **C**), cross-linked electrospun GE:PLLA 1:1 containing 1% w of HA (+1% HA, **D**), cross-linked electrospun GE:PLLA1:1 containing 1.5% w of HA (+1.5% HA, **E**), and cross-linked electrospun GE:PLLA 1:1 containing 2% w of HA (+2% HA, **F**). **(G)** Mean fluorescence lifetime (τ_m) after two-photon excitation at 710 nm of electrospun collagen, cross-linked electrospun GE:PLLA 1:1, cross-linked electrospun GE:PLLA 1:1 containing 0.5% w of HA (+0.5% HA), cross-linked electrospun GE:PLLA 1:1 containing 1% w of HA (+1% HA), cross-linked electrospun GE:PLLA1:1 containing 1.5% w of HA (+1.5% HA), and cross-linked electrospun GE:PLLA 1:1 containing 2% w of HA (+2% HA). A shift toward shorter τ_ms was detected with the increasing HA percentage in the scaffolds.

time hypothesized that HA only helps to treat the symptoms associated with pathological conditions, it is well accepted that HA directly affects cell metabolism especially under oxidative stress by improving the cell's mitochondrial function and enhancing cell survival.[101–103,108,109]

Particularly, it has been demonstrated that HA sustains mitochondrial DNA repair capacity, preserves normal cellular ATP levels, inhibits inflammatory responses, and eventually prevents apoptotic events.[101,110–112] Considering this, and according to our own results, we believe that the presence of HA exerts regulatory effects on the HDFs seeded on the hybrid scaffolds preserving their mitochondrial function. As a consequence, using FLIM, we could observe a significant decrease in the free NAD(P)H α_1 (%) ratio of HDFs seeded on the HA-containing hybrid scaffolds due to a higher contribution of the mitochondrial NAD(P)H when compared with the HDFs seeded on glass, collagen type I, or not functionalized GE:PLLA scaffolds.

Conclusion

In this study, we described the production of hybrid GE:PLLA electrospun scaffolds whose hydrophilicity was modified by cross-linking specific amounts of HA to the free amine residues of GE. Interestingly, these manufactured 3D scaffolds showed an SHG signal pattern that is comparable to the SHG pattern of native collagen fibers. Profiting from the SHG signal and the natural endogenous autofluorescence of GE, we were able to marker independently and non-invasively image the electrospun scaffolds either alone or after the seeding of HDFs.

FLIM further enabled us to distinguish and separate the scaffold fiber signals from that of the cellular NAD(P)H, which was chosen as an endogenous target. We analyzed the ratio of the free glycolytic NAD(P)H in the HDFs and investigated metabolic changes in these cells. The here presented data are highly relevant when aiming for the simultaneous *in vitro* imaging and metabolic analysis of

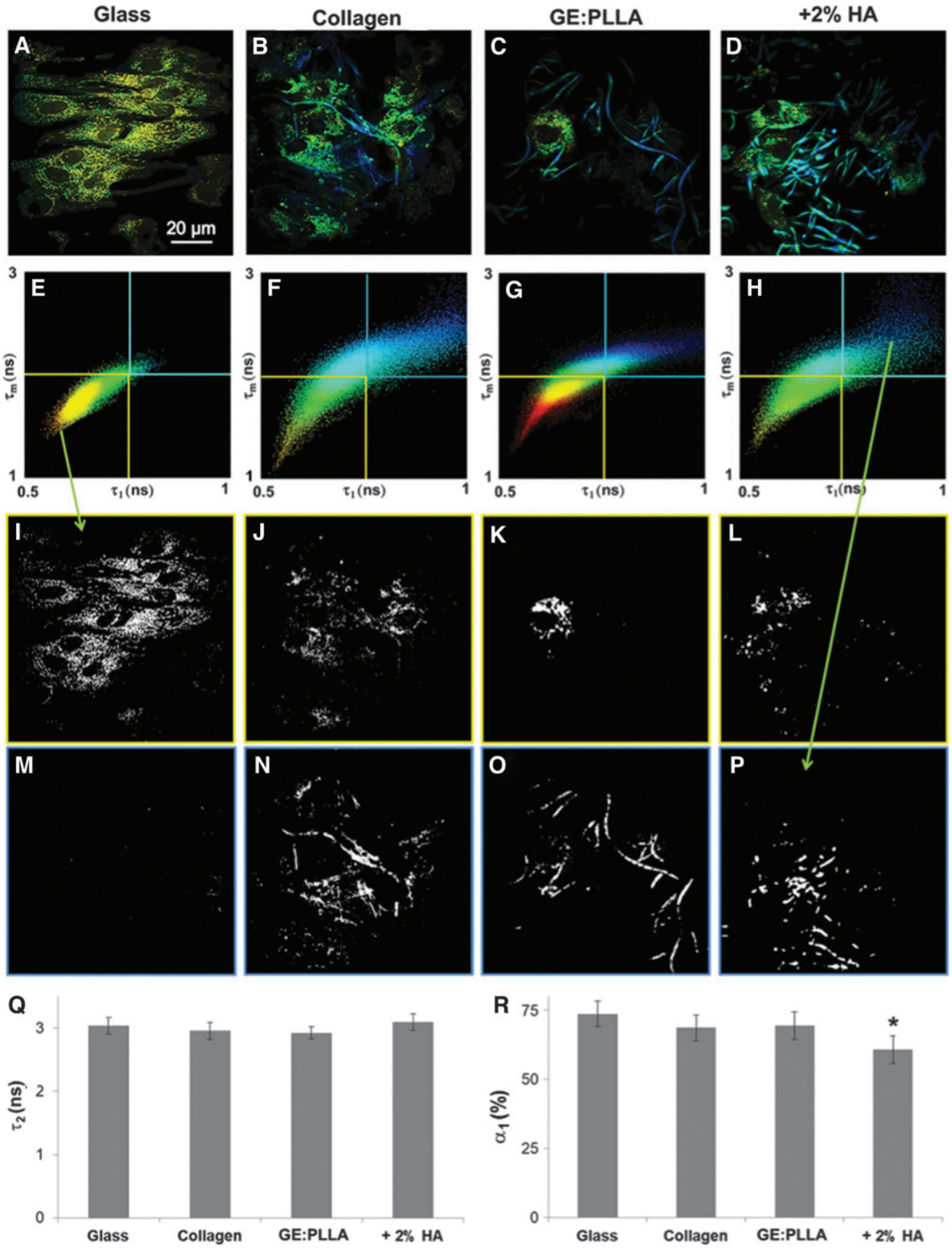

FIG. 7. **(A–D)** FLIM false color-coded imaging of HDFs seeded on glass **(A)**, electrospun collagen **(B)**, hybrid cross-linked GE:PLLA 1:1 **(C)**, and cross-linked GE:PLLA 1:1 with 2% w HA (+2% HA, **D**). **(E–H)** 2D correlation between τ_1 and τ_m after biexponential decay curve fitting of the FLIM data. **(I–L)** Pixels occupying the *left*-down quarter of the 2D correlation ($\tau_1 < 0.75$ ns and $\tau_m < 2$ ns). **(M–P)** Pixels occupying the *right*-up quarter of the 2D correlation ($\tau_1 > 0.75$ ns and $\tau_m > 2$ ns). **(Q)** Mean values for protein bound NAD(P)H fluorescence lifetime τ_2. **(R)** Mean values for the ratio of glycolytic NAD(P)H α_1%. $^*p \leq 0.05$ is significant. 2D, two-dimensional; FLIM, fluorescence lifetime imaging microscopy; HDFs, human dermal fibroblasts. Color images are available online.

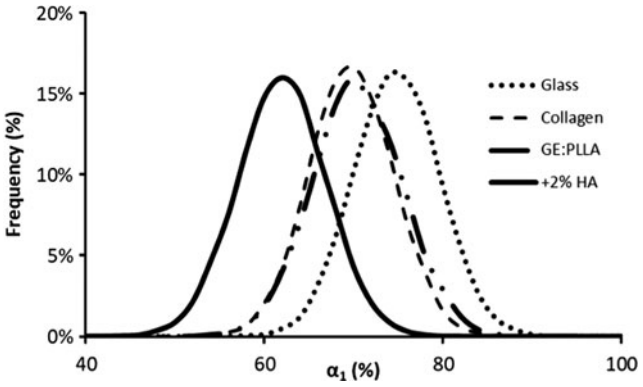

FIG. 8. Histograms for the distribution of the $\alpha_1\%$ values [Eq. (4)], where $\alpha_1\% = \alpha_1/(\alpha_1 + \alpha_2)$ represents the free NADP(H) ratio of HDFs cultured on different surfaces.

cultured cells in an environment close to the physiological one, which is crucial for the *in vitro* testing of drugs, metabolites, and other bioactive molecules.

Acknowledgments

The authors thank Simone Liebscher (University Hospital Tübingen, Germany) and Donato Pace (Ripa SAS, Potenza, Italy) for their technical support, and Eva M. Brauchle (University Hospital Tübingen, Germany) for advice with the Raman microspectrocopical analyses.

Disclosure Statement

No competing financial interests exist.

Funding Information

The authors are grateful for the financial support by the DAAD (Year scholarship program 57130104 to G.P.), as well as the State Ministry for Science, Research, and the Arts of Baden-Württemberg (33–729.55-3/214 and SI-BW 01222-91 to K.S.-L.), the State Ministry for Economic Affairs, Labour and Tourism of Baden-Württemberg, and the Deutsche Forschungsgemeinschaft (EXC 2180-390900677 to K.S.-L.).

References

1. Heydarkhan-Hagvall, S., Schenke-Layland, K., Dhanasopon, A.P., *et al.* Three-dimensional electrospun ECM-based hybrid scaffolds for cardiovascular tissue engineering. Biomaterials **29,** 2907, 2008.
2. Wang, X., Ding, B., and Li, B. Biomimetic electrospun nanofibrous structures for tissue engineering. Mater Today **16,** 229, 2013.
3. Liu, W., Thomopoulos, S., and Xia, Y. Electrospun nanofibers for regenerative medicine. Adv Healthc Mater **1,** 10, 2012.
4. Lyu, S., Huang, C., Yang, H., and Zhang, X. Electrospun fibers as a scaffolding platform for bone tissue repair. J Orthop Res **31,** 1382, 2013.
5. Bonvallet, P.P., Schultz, M.J., and Mitchell, E.H., *et al.* Microporous dermal-mimetic electrospun scaffolds preseeded with fibroblasts promote tissue regeneration in full-thickness skin wounds. PLoS One **10,** e0122359, 2015.
6. Gunn, J., and Zhang, M. Polyblend nanofibers for biomedical applications: perspectives and challenges. Trends Biotechnol **28,** 189, 2010.
7. Bhattarai, N., Li, Z., Gunn, J., *et al.* Natural-synthetic polyblend nanofibers for biomedical applications. Adv Mater **21,** 2792, 2009.
8. Espíndola-González, A., Martínez-Hernández, A.L., Fernández-Escobar, F., *et al.* Natural-synthetic hybrid polymers developed via electrospinning: the effect of PET in chitosan/starch system. Int J Mol Sci **12,** 1908, 2011.
9. Martinova, L., and Lubasova, D. Reasons for using polymer blends in the electrospinning process. AIP Conf Proc **1502,** 115, 2012.
10. Tipduangta, P., Belton, P., Fábián L, *et al.* Electrospun polymer blend nanofibers for tunable drug delivery: the role of transformative phase separation on controlling the release rate. Mol Pharm **13,** 25, 2016.
11. Khajavi, R., and Abbasipour, M. Electrospinning as a versatile method for fabricating coreshell, hollow and porous nanofibers. Sci Iran **19,** 2029, 2012.
12. Kishan, A.P., and Cosgriff-Hernandez, E.M. Recent advancements in electrospinning design for tissue engineering applications: a review. J Biomed Mater Res A **105,** 2892, 2017.
13. Lee, G.H., Song, J.C., and Yoon, K.B. Controlled wall thickness and porosity of polymeric hollow nanofibers by coaxial electrospinning. Macromol Res **18,** 571, 2010.
14. Loh, Q.L., and Choong, C. Three-dimensional scaffolds for tissue engineering applications: role of porosity and pore size. Tissue Eng Part B Rev **19,** 485, 2013.
15. Sundararaghavan, H.G., Metter, R.B., and Burdick, J.A. Electrospun fibrous scaffolds with multi-scale and photopatterned porosity. Macromol Biosci **10,** 265, 2010.
16. Rnjak-Kovacina, J., and Weiss, A.S. Increasing the pore size of electrospun scaffolds. Tissue Eng Part B Rev **17,** 365, 2011.
17. Blakeney, B.A., Tambralli, A., Anderson, J.M., *et al.* Cell infiltration and growth in a low density, uncompressed three-dimensional electrospun nanofibrous scaffold. Biomaterials **32,** 1583, 2011.
18. Pham, Q.P., Sharma, U., and Mikos, A.G. Electrospinning of polymeric nanofibers for tissue engineering applications: a review. Tissue Eng **12,** 1197, 2006.
19. Greiner, A., and Wendorff, J.H. Electrospinning: a fascinating method for the preparation of ultrathin fibers. Angew Chem Int Ed Engl **46,** 5670, 2007.
20. Xiao, L., Wang, B., Yang, G., and Gauthier, M. Poly (lactic acid)-based biomaterials: synthesis, modification and applications. In: Ghista, D.N., ed. Biomedical Science, Engineering and Technology. London, UK: IntechOpen, 2012, p. 247. DOI: 10.5772/23927.
21. Cheng, Y., Deng, S., Chen, P., and Ruan, R. Polylactic acid (PLA) synthesis and modification: a review. Front Chem China **4,** 259, 2009.
22. Gupta, B., Revagade, N., and Hilborn, J. Poly(lactic acid) fiber: an overview. Prog Polym Sci **32,** 455, 2007.
23. Boland, E.D., Wnek, G.E., Simpson, D.G., Pawlowski, K.J., and Bowlin, G.L. Tailoring tissue engineering scaffolds using electrostatic processing techniques: a study of poly (glycolic acid) electrospinning. J Macromol Sci A **38,** 1231, 2001.
24. Gentile, P., Chiono, V., Carmagnola, I., and Hatton, P.V. An overview of poly(lactic-co-glycolic) acid (PLGA)-based biomaterials for bone tissue engineering. Int J Mol Sci **15,** 3640, 2014.

25. Dong, Y., Liao, S., Ngiam, M., Chan, C.K., and Ramakrishna, S. Degradation behaviors of electrospun resorbable polyester nanofibers. Tissue Eng Part B Rev **15,** 333, 2009.
26. Liu, H., Wang, S., and Qi, N. Controllable structure, properties, and degradation of the electrospun PLGA/PLA-blended nanofibrous scaffolds. J Appl Polym Sci **125,** E468, 2012.
27. Matthews, J.A., Wnek, G.E., Simpson, D.G., and Bowlin, G.L. Electrospinning of collagen nanofibers. Biomacromolecules **3,** 232, 2002.
28. Li, M., Mondrinos, M.J., Gandhi, M.R., Ko, F.K., Weiss, A.S., and Lelkes, P.I. Electrospun protein fibers as matrices for tissue engineering. Biomaterials **26,** 5999, 2005.
29. Schiffman, J.D., and Schauer, C. A review: electrospinning of biopolymer nanofibers and their applications. Polym Rev **48,** 317, 2008.
30. Dang, J.M., and Leong, K.W. Natural polymers for gene delivery and tissue engineering. Adv Drug Deliv Rev **58,** 487, 2006.
31. Kwon, K., and Matsuda, T. Co-electrospun nanofiber fabrics of poly(l-lactide-co-ε-caprolactone) with type I collagen or heparin. Biomacromolecules **6,** 2096, 2005.
32. Zhang, Y., Su, B., Venugopal, J., Ramakrishna, S., and Lim, C. Biomimetic and bioactive nanofibrous scaffolds from electrospun composite nanofibers. Int J Nanomed **2,** 623, 2007.
33. Eastoe, J.E. The amino acid composition of mammalian collagen and gelatin. Biochem J **61,** 589, 1955.
34. Jones, R.T. Gelatin: manufacture and physio-chemical properties. In: Podczeck, F., and Jones, B.E., eds. Pharmaceutical Capsules. London, UK: Pharmaceutical Press, 2004, p. 23.
35. Katagiri, Y., Brew, S.A., and Ingham, K.C. All six modules of the gelatin-binding domain of fibronectin are required for full affinity. J Biol Chem **278,** 11897, 2003.
36. Tondera, C., Hauser, S., Krüger-Genge, A., *et al.* Gelatin-based hydrogel degradation and tissue interaction in vivo: insights from multimodal preclinical imaging in immunocompetent nude mice. Theranostics **6,** 2114, 2016.
37. Lai, J.Y. Biocompatibility of chemically cross-linked gelatin hydrogels for ophthalmic use. J Mater Sci Mater Med **21,** 1899, 2010.
38. De la Mata, A., Nieto-Miguel, T., López-Paniagua, M., *et al.* Chitosan-gelatin biopolymers as carrier substrata for limbal epithelial stem cells. J Mater Sci Mater Med **24,** 2819, 2013.
39. Tonsomboon, K., Strange, D.G.T., and Oyen, M.L. Gelatin nanofiber-reinforced alginate gel scaffolds for corneal tissue engineering. Proc Eng Med Biol Soc **1,** 6671, 2013.
40. Bohidar, H.B., and Jena, S.S. Study of sol-state properties of aqueous gelatin solutions. J Chem Phys **100,** 6888, 1994.
41. Rose, J.B., Pacelli, S., Haj, A.J.E., *et al.* Gelatin-based materials in ocular tissue engineering. Materials **7,** 3106, 2014.
42. Tomihata, K., and Ikada, Y. Cross-linking of gelatin with carbodiimides. Tissue Eng **2,** 307, 2007.
43. Sisson, K., Zhang, C., Farach-Carson, M.C., Chase, D.B., and Rabolt, J.F. Evaluation of cross-linking methods for electrospun gelatin on cell growth and viability. Biomacromolecules **10,** 1675, 2009.
44. Digenis, G.A., Gold, T.B., and Shah, V.P. Cross-linking of gelatin capsules and its relevance to their in vitro-in vivo performance. J Pharm Sci **83,** 915, 1994.
45. Collins, M.N., and Birkinshaw, C. Comparison of the effectiveness of four different crosslinking agents with hyaluronic acid hydrogel films for tissue-culture applications. J Appl Polym Sci **104,** 3183, 2007.
46. Cammarata, C.R., Hughes, M.E., and Ofner, C.M. Carbodiimide induced cross-linking, ligand addition, and degradation in gelatin. Mol Pharm **12,** 783, 2015.
47. Zhou, Z., Yang, Z., Huang, T., *et al.* Effect of chemical cross-linking on properties of gelatin/hyaluronic acid composite hydrogels. Polym Plast Technol Eng **52,** 45, 2013.
48. Jarquín-Yáñez, K., Arenas-Alatorre, J., Piñón-Zárate, G., *et al.* Structural effect of different EDC crosslinker concentration in gelatin hyaluronic acid scaffolds. J Bioeng Biomed Sci **6,** e1000182, 2016.
49. Lou, X., and Chirila, T. Swelling behaviour and mechanical properties of chemically cross-linked gelatin gels for biomedical use. J Biomater Appl **14,** 184, 1999.
50. Raquez, J.M., Mincheva, R., Coulembier, O., and Dubois, P. Polymer Science: A Comprehensive Reference. **Vol. 1**. Amsterdam, Netherlands: Elsevier, 2012, p. 761.
51. Park, K., Ju, Y.M., Son, J.S., Ahn, K., and Han, D.K. Surface modification of biodegradable electrospun nanofiber scaffolds and their interaction with fibroblasts. J Biomater Sci Polym Ed **18,** 369, 2007.
52. Aoki, M., Miyamoto, S., Okamura, K., Yamashita, T., Ikada, Y., and Matsuda, S. Tensile properties and biological response of poly(L-lactic acid) felt graft: an experimental trial for rotator-cuff reconstruction. J Biomed Mater Res **71B,** 252, 2004.
53. Groot, W., Van Krieken, J., Sliekersl, O., and De Vos, S. Production and purification of lactic acid and lactide. In: Auras, R., Lim, L., Selke, S., and Tsuji, H., eds. Poly(Lactic Acid): Synthesis, Structures, Properties, Processing, and Applications. Weinheim, Germany: Wiley-VCH, 2010, p. 1.
54. Södergård, A., and Stolt, M. Industrial production of high molecular weight poly(lactic acid). In: Auras, R., Lim, L., Selke, S., and Tsuji, H., eds. Poly(Lactic Acid): Synthesis, Structures, Properties, Processing, and Applications. Weinheim, Germany: Wiley-VCH, 2010, p. 27.
55. Lee, S.H., and Song, W.S. Enzymatic hydrolysis of polylactic acid fiber. Appl Biochem Biotechnol **164,** 89, 2011.
56. Necas, J., Bartosikova, L., Brauner, P., and Kolar, J. Hyaluronic acid (hyaluronan): a review. Vet Med **53,** 397, 2008.
57. Kim, T.G., Chung, H.J., and Park, T.G. Macroporous and nanofibrous hyaluronic acid/collagen hybrid scaffold fabricated by concurrent electrospinning and deposition/leaching of salt particles. Acta Biomater **4,** 1611, 2008.
58. Chen, W.Y.J., and Abatangelo, G. Functions of hyaluronan in wound repair. Wound Repair Regen **7,** 79, 1999.
59. Chen, W., Chen, S., Morsi, Y., *et al.* Superabsorbent 3D scaffold based on electrospun nanofibers for cartilage tissue engineering. ACS Appl Mater Interfaces **8,** 24415, 2016.
60. Matou-Nasri S, Gaffney J, Kumar, S., and Slevin, M. Oligosaccharides of hyaluronan induce angiogenesis through distinct CD44 and RHAMM-mediated signaling pathways involving Cdc2 and gamma-adducin. Int J Oncol **35,** 761, 2009.
61. Frantz, C., Stewart, K.M., and Weaver, V.M. The extracellular matrix at a glance. J Cell Sci **123,** 4195, 2010.

62. Papakonstantinou, E., Roth, M., and Karakiulakis, G. Hyaluronic acid: a key molecule in skin aging. Dermatoendocrinol **4,** 253, 2012.
63. Nishimura, I., Garrell, R.L., Hedrick, M., Iida, K., Osher, S., and Wu, B. Precursor tissue analogs as a tissue-engineering strategy. Tissue Eng **9,** S77, 2003.
64. Kherlopian, A.R., Song, T., Duan, Q., *et al.* A review of imaging techniques for systems biology. BMC Syst Biol **2,** 74, 2008.
65. Schenke-Layland, K. Non-invasive multiphoton imaging of extracellular matrix structures. J Biophotonics **1,** 451, 2008.
66. Hinderer, S., Brauchle, E., and Schenke-Layland, K. Generation and assessment of functional biomaterial scaffolds for applications in cardiovascular tissue engineering and regenerative medicine. Adv Healthc Mater **4,** 2326, 2015.
67. Benninger, R.K.P., and Piston, D.W. Two-photon excitation microscopy for the study of living cells and tissues. Curr Protoc Cell Biol **Chapter 4**, Unit 4.11.1, 2013.
68. Balu, M., Zachary, C.B., Harris, R.M., *et al.* In vivo multiphoton microscopy of basal cell carcinoma. JAMA Dermatol **151,** 1068, 2015.
69. Brockbank, K.G.M., MacLellan, W.R., Xie, J.S., Hamm-Alvarez, S.F., Chen, Z.Z., and Schenke-Layland, K. Quantitative second harmonic generation imaging of cartilage damage. Cell Tissue Bank **9,** 299, 2008.
70. Hinderer, S., Schesny, M., Bayrak, A., *et al.* Engineering of fibrillar decorin matrices for a tissue-engineered trachea. Biomaterials **33,** 5259, 2012.
71. Dong, B., Arnoult, O., Smith, M.E., and Wnek, G.E. Electrospinning of collagen nanofiber scaffolds from benign solvents. Macromol Rapid Commun **30,** 539, 2009.
72. Yang, X.X., Wang, X.Y., Yu, F., *et al.* Hyaluronic acid/EDC/NHS-crosslinked green electrospun silk fibroin nanofibrous scaffolds for tissue engineering. RSC Adv **6,** 99720, 2016.
73. Vangara, K.K., Liu, J.L., and Palakurthi, S. Hyaluronic acid-decorated PLGA-PEG nanoparticles for targeted delivery of SN-38 to ovarian cancer. Anticancer Res **33,** 2425, 2013.
74. Qhattal, H.S., and Liu, X. Characterization of CD44-mediated cancer cell uptake and intracellular distribution of hyaluronangrafted liposomes. Mol Pharm **8,** 1233, 2011.
75. Hinderer, S., Seifert, J., Votteler, M., *et al.* Engineering of a bio-functionalized hybrid off-the-shelf heart valve. Biomaterials **35,** 2130, 2014.
76. Tan, Q., Li, S., Ren, J., and Chen, C. Fabrication of porous scaffolds with a controllable microstructure and mechanical properties by porogen fusion technique. Int J Mol Sci **12,** 890, 2011.
77. Brauchle, E., Johannsen, H., Nolan, S., Thude, S., and Schenke-Layland, K. Design and analysis of a squamous cell carcinoma in vitro model system. Biomaterials **34,** 7401, 2013.
78. Kluger, P.J., Wyrwa, R., Weisser, J., *et al.* Electrospun poly(D/L-lactide-co-L-lactide) hybrid matrix: a novel scaffold material for soft tissue engineering. J Mater Sci Mater Med **21,** 2665, 2010.
79. Pudlas, M., Koch, S., Bolwien, C., *et al.* Raman spectroscopy: a non invasive analysis tool for the discrimination of human skin cells. Tissue Eng Part C Methods **17,** 1027, 2011.
80. Lakner, P.H., Monaghan, M.G., Möller, Y., Olayioye, M.A., and Schenke-Layland, K. Applying phasor approach analysis of multiphoton FLIM measurements to probe the metabolic activity of three-dimensional in vitro cell culture models. Sci Rep **7,** 42730, 2017.
81. Lin, S., Wu, R., Tan, H., *et al.* Evaluating cutaneous photoaging by use of multiphoton fluorescence and second-harmonic generation microscopy. Opt Lett **30,** 2275, 2005.
82. Scott, T.G., Spencer, R.D., Leonard, N.J., and Weber, G. Synthetic spectroscopic models related to coenzymes and base pairs. V. Emission properties of NADH. Studies of fluorescence lifetimes and quantum efficiencies of NADH, AcPyADH, [reduced acetylpyridineadenine dinucleotide] and simplified synthetic models. J Am Chem Soc **92,** 687, 1970.
83. Essendoubi, M., Gobinet, C., Reynaud, R., Angiboust, J.F., Manfait, M., and Piot, O. Human skin penetration of hyaluronic acid of different molecular weights as probed by Raman spectroscopy. Skin Res Technol **22,** 55, 2016.
84. Barrett, T.W., and Peticolas, W.L. Laser Raman inelastic light scattering investigations of hyaluronic acid primary and secondary structure. J Raman Spectrosc **8,** 35, 1979.
85. Kotzianova, A., Rebicek, J., Zidek, O., Pokorny, M., Hrbac, J., and Velebny, V. Raman spectroscopy based method for the evaluation of compositional consistency of nanofibrous layers. Anal Methods **7,** 9900, 2015.
86. Kister, G., Cassanas, G., and Vert, M. Effects of morphology, conformation and configuration on the IR and Raman spectra of various poly(lactic acid)s. Polymer **39,** 267, 1998.
87. Qin, D., and Kean, R. Crystallinity, determination of polylactide by FT-Raman spectrometry. Appl Spectrosc **52,** 488, 1998.
88. Vano-Herrera, K., and Vogt, C. Degradation of poly(L-lactic acid) coating on permanent coronary metal stent investigated ex vivo by micro Raman spectroscopy. J Raman Spectrosc **48,** 711, 2017.
89. Piccirillo, G., Ditaranto, M.V., Feuerer, N.F.S., *et al.* Non-invasive characterization of hybrid gelatin: poly-L-lactide electrospun scaffolds with controlled structural properties using second harmonic generation and multiphoton imaging. J Mater Chem B **6,** 6399, 2018.
90. Zeugolis, D.I., Khew, S.T., Yew, E.S., *et al.* Electrospinning of pure collagen nano-fibres—just an expensive way to make gelatin? Biomaterials **29,** 2293, 2008.
91. Schrimpf, W., Ossato, G., Hirschle, P., Wuttke, S., and Lamb, D.C. Investigation of the Co-dependence of morphology and fluorescence lifetime in a metal-organic framework. Small **12,** 3651, 2016.
92. Wang, W., Li, J., Duan, G., Zhao, W., Cao, B., and Liu, Z. Morphology/size effect on the luminescence properties of the [(Y x Gd 1-x) 0.98 Dy 0.02] 2 O 3 phosphor with enhanced yellow emission. J Lumin **192,** 1056, 2017. DOI: 10.1016/j.jlumin.2017.07.046.
93. Yu, H., Wang, H., Li, Y., *et al.* Electrospinning preparation and luminescence properties of terbium complex/polymer composite fibers. J Nanosci Nanotechnol **14,** 3914, 2014.
94. Fukushima, S., Shimizu, M., Miura, J., *et al.* Decrease in fluorescence lifetime by glycation of collagen and its application in determining advanced glycation end-products in human dentin. Biomed Opt Express **6,** 1844, 2015.
95. Lai, J.Y., Ma, D.H.K., Lai, M.H., Li, Y.T., Chang, R.J., and Chen, L. Characterization of cross-linked porous gelatin carriers and their interaction with corneal endothelium: biopolymer concentration effect. PLoS One **8,** e54058, 2013.

96. Nguyen, T.H., and Lee, B.T. The effect of cross-linking on the microstructure, mechanical properties and biocompatibility of electrospun polycaprolactone–gelatin/PLGA–gelatin/PLGA–chitosan hybrid composite. Sci Technol Adv Mater **13,** 035002, 2012.
97. Nguyen, T.H., and Lee, B.T. Fabrication and characterization of cross-linked gelatin electrospun nano-fibers. J Biomed Sci Eng **3,** 1117, 2010.
98. Blacker, T.S., Mann, Z.F., Gale, J.E., *et al.* Separating NADH and NADPH fluorescence in live cells and tissues using FLIM. Nat Commun **5,** 3936, 2014.
99. Piccirillo, G., Bochicchio, B., Pepe, A., Schenke-Layland, K., and Hinderer, S. Electrospun poly-l-lactide scaffold for the controlled and targeted delivery of a synthetically obtained Diclofenac prodrug to treat actinic keratosis. Acta Biomater **52,** 187, 2017.
100. Seidenari, S., Arginelli, F., Dunsby, C., *et al.* Multiphoton laser tomography and fluorescence lifetime imaging of melanoma: morphologic features and quantitative data for sensitive and specific non-invasive diagnostics. PLoS One **8,** e70682, 2013.
101. Grishko, V., Xu, M., Ho, R., *et al.* Effects of hyaluronic acid on mitochondrial function and mitochondria-driven apoptosis following oxidative stress in human chondrocytes. J Biol Chem **14,** 9132, 2009.
102. Solis, M.A., Chen, Y., Wong, T.Y., *et al.* Hyaluronan regulates cell behavior: a potential niche matrix for stem cells. Biochem Res Int **2012,** 346972, 2012.
103. Grishko, V., Pearsall, A.W., and Wilson, G. Chondroprotective effects of hyaluronic acid following oxidative stress. Arthroscopy **23,** e25, 2007.
104. Masuko, K., Murata, M., Yudoh, K., Kato, T., and Nakamura, H. Anti-inflammatory effects of hyaluronan in arthritis therapy: not just for viscosity. Int J Gen Med **2,** 77, 2009.
105. Litwiniuk, M., Krejner, A., Speyrer, M.S., Gauto, A.R., and Grzela, T. Hyaluronic acid in inflammation and tissue regeneration. Wounds **28,** 78, 2016.
106. Liao, Y., Jones, S.A., Forbes, B., Martin, G.P., and Brown, M.B. Hyaluronan: pharmaceutical characterization and drug delivery. Drug Deliv **12,** 327, 2005.
107. Voigt, J., and Vickie, D. Hyaluronic acid derivatives and their healing effect on burns, epithelial surgical wounds, and chronic wounds: a systemic review and meta-analysis of randomized controlled trials. Wound Repair Regen **20,** 317, 2012.
108. Viola, M., Vigetti, D., Karousou, E., *et al.* Biology and biotechnology of hyaluronan. Glycoconj J **32,** 93, 2015.
109. Genasetti, A., Vigetti, D., Viola, M., *et al.* Hyaluronan and human endothelial cell behavior. Connect Tissue Res **49,** 120, 2008.
110. Barreto, R.B., Sadigursky, D., de Rezende, M.U., and Hernandez, A.J. Effect of hyaluronic acid on chondrocyte apoptosis. Acta Ortop Bras **23,** 90, 2015.
111. Kaneko, T., Saito, H., Toya, M., Satio, T., Nakahara, K., and Hiroi, M. Hyaluronic acid inhibits apoptosis in granulosa cells via CD44. J Assist Reprod Genet **17,** 162, 2000.
112. Peng, H., Zhou, J., Liu, S., Hu, Q., Ming, J., and Qiu, B. Hyaluronic acid inhibits nitric oxide-induced apoptosis and dedifferentiation of articular chondrocytes *in vitro*. Inflamm Res **59,** 519, 2010.

Address correspondence to:
Katja Schenke-Layland, PhD
Institute of Biomedical Engineering
Department for Medical Technologies
and Regenerative Medicine
Eberhard Karls University Tübingen
Silcherstr. 7/1
Tübingen 72076
Germany

E-mail: katja.schenke-layland@uni-tuebingen.de

Received: September 23, 2021
Accepted: October 18, 2021
Online Publication Date: November 17, 2021